



## Shifting Mineral and Redox Controls on Carbon Cycling in Seasonally Flooded Soils

5 Rachel LaCroix<sup>1</sup>, Malak Tfaily<sup>2</sup>, Menli McCreight<sup>1</sup>, Morris E. Jones<sup>1</sup>, Lesley Spokas<sup>1</sup>, and Marco Keiluweit<sup>1,\*</sup>

<sup>1</sup>School of Earth & Sustainability and Stockbridge School of Agriculture, University of Massachusetts, Amherst, MA-01003, United States

<sup>2</sup>Environmental Molecular Sciences Laboratory, Pacific Northwest National Laboratory, Richland, WA-99354, United States

*Correspondence to:* Marco Keiluweit ([keiluweit@umass.edu](mailto:keiluweit@umass.edu))

10 **Abstract.** Soils contain three times the amount of carbon (C) than the atmosphere, with C turnover times ranging from centuries to millennia. Although wetland soils represent a relatively small portion of the terrestrial landscape, they account for an estimated 20-30% of the global C reservoir. Among wetlands, seasonally flooded soils are likely the most vulnerable to increased severity and duration of droughts in response to climate change. Yet, the relative influence of associated changes in oxygen limitations, root dynamics, and mineral protection on C cycling in seasonally flooded mineral soils is largely unknown.

15 To address this knowledge gap, we combined seasonal monitoring of soil moisture, redox potential, and CO<sub>2</sub> efflux with a characterization of root biomass, mineralogy, C quantity and organic matter composition along upland-to-lowland transects of both top- and subsoils in temperate forested wetlands. We found that lower CO<sub>2</sub> effluxes in lowland than upland topsoils coincided with greater total C concentrations as well as a greater abundance of high molecular weight and chemically reduced organic compounds, indicating that selective preservation of organic compounds during anaerobic periods caused C

20 accumulation in seasonally flooded surface soils. In subsoils, however, seasonal flooding and associated anaerobic conditions did not result in soil C accumulation. Instead, total C concentrations were significantly lower in lowland than in upland subsoils. Lower soil C accumulation in seasonally flooded subsoils coincided with lower abundance of root biomass and reducible Fe phases, and relied primarily on non-reducible Al phases rather than anaerobic conditions. Combined, our results demonstrate that seasonal flooding and associated anaerobic conditions accumulate C in topsoils, but limit C accumulation in

25 subsoils by restricting root C inputs and removing of protective Fe phases through reductive dissolution. Our findings indicate that C accrual in seasonally flooded soil is due primarily to oxygen limitations in the surface soil, and that the overall lack of mineral protection leaves these C stocks highly vulnerable to climate change.



## 1 Introduction

Although wetland soils cover a relatively small portion of the Earth's land surface, they store an estimated 20-30% of the global soil C stocks (Mitsch et al., 2013). However, this C pool is under pressure from climate change, with increasing severity and frequency of droughts having substantial, yet largely unresolved consequences (Brooks et al., 2009, Fenner and Freeman, 2011). Increased droughts are expected to release previously stored C in wetlands back into the atmosphere (Gorham et al., 1991). Prior studies focused on C cycling in wetland soils have been primarily aimed at organic wetlands, such as peats and bogs (Laine et al., 1996) or coastal wetlands (Kirwan and Blum, 2011). Although freshwater mineral wetlands are estimated to contain 46 Pg C globally (Bridgham et al., 2006), they have received comparatively little attention.

Previous studies on C cycling in mineral wetland soils are limited to permanently flooded, rather than seasonally flooded sites (Krauss and Whitbeck, 2012). This is surprising given that seasonally flooded soils are metabolically more active than permanently flooded wetlands, resulting in significantly greater greenhouse gas emissions (Kifner et al. 2018). Moreover, the consequences of climate change is expected to be most immediately evident in seasonal wetlands due to their dependence upon precipitation and seasonal groundwater recharge (Tiner, 2003). Seasonal wetlands are considered as early warning and detection ecosystems (Brooks, 2005); forecasting the impacts of climate change on permanently flooded mineral wetlands. Thus, seasonally flooded wetlands are ideal model ecosystems to study the effects of climate change on larger permanently flooded wetland soils (Brooks, 2005).

Seasonal wetlands are geomorphic depressions in the landscape that have distinct hydrologic phases of flooding and draining (Brooks, 2005). These ephemeral wetlands are small (<1 hectare), but ubiquitous – comprising nearly 70% of all temperate forest wetlands in the US (Tiner, 2003). Seasonal flooding and drainage not only creates biogeochemical “hotspots” for soil C and nutrient cycling along upland-to-lowland transitions, but also “hot moments” as these transition zones move seasonally (Cohen et al., 2016). These transition zones are also relatively large, as the generally small size of seasonal wetlands results in a disproportionately large and dynamic terrestrial-aquatic interface relative to total wetland area (Cohen et al., 2016). Determining the controls on C cycling within seasonally flooded mineral soils thus requires specific consideration of the fluxes and dynamics across these terrestrial-aquatic transitions.



Though temperature and soil moisture are principle controls on C cycling in soils generally (Lloyd and Taylor, 1994; Wang et al., 2014), water saturation is a critically driver of soil organic matter (OM) decomposition processes in seasonally flooded systems (Neckles and Niell, 1994). Water saturation governs oxygen availability in soil pore spaces, as oxygen diffusion in water is 10,000 times slower than in air (Letey and Stolzy, 1964). The resulting oxygen limitations inhibit the activity of oxidative enzymes catalyzing the depolymerization of higher-molecular weight OM into smaller, assimilable compounds (Megonigal et al. 2003). Further, once oxygen is depleted, microbes rely on alternative terminal electron acceptors ( $\text{NO}_3^-$ ,  $\text{Mn}^{4+}$ ,  $\text{Fe}^{3+}$ ,  $\text{SO}_4^{2-}$ ) in heterotrophic respiration that yield less energy (Sutton-Grier et al., 2011). These thermodynamic constraints also dictate the types of organic substrate microbes are able to use in heterotrophic respiration (LaRowe and Van Cappellen, 2011). Anaerobic conditions limit microbes to utilizing substrates that are chemically more oxidized, in turn preferentially preserving more chemically-reduced organic compounds in soils and sediments (Boye et al. 2017; Keiluweit et al., 2017). While  $\text{CO}_2$  emissions are often correlated with oxygen availability (or soil redox potential) (Koh et al., 2009), it is unclear to what extent such metabolic constraints result in the selective preservation of high-molecular weight, chemically-reduced OM in seasonally flooded systems where soils become aerated for prolonged periods.

Water saturation also impacts soil by controlling vegetation type and density – thus acting as an indirect control on root growth and activity belowground. Plant roots contribute to soil C stocks through active rhizodeposition (exudates, secretions, dead border cells, and mucilages), dead root residues (Jones et al., 2009), and root-associated microbes (Bradford et al., 2013). Roots are the main contributors to C stocks in upland soils (Rasse et al., 2005), but root impacts on soil C stocks in wetlands is less clear. Water saturation directly inhibits root growth due to the associated low redox potentials (Day and Megonigal, 1993; Tokarz and Urban, 2015). Indirectly, water saturation in soil selects for plant species that can tolerate water stress – typically species that have developed advantageous traits to survive flooded conditions, such as shallow rooting systems (Tokarz and Urban, 2015). However, seasonally flooded soils select for an even smaller niche of plants, as they must be tolerant of both upland and lowland conditions (Brooks, 2005). How root inputs from facultative upland-to-lowland plant species contribute to soil C content and chemistry in seasonally flooded soils is still not clear.

In addition to restricting microbial metabolism and root growth, water saturation also influences the concentration and distribution of reactive minerals that contribute to C accumulation in soils (Chen et al., 2017; Torn et al., 1997; Wagai and



Mayer, 2007). In upland soils, iron (Fe) or aluminum (Al) (hydr)oxides protect OM from microbial decomposition, thereby contributing to C storage for centuries to millennia (Torn et al., 1997; Wagai and Mayer, 2007). In flooded soils, however, the rapid depletion of oxygen upon flooding can result in the reductive dissolution of Fe(III) oxides (Chen et al., 2017), potentially causing the mobilization of previously Fe-bound OM (Zhao et al., 2017). During water table drawdown, Fe(II) may be leached  
5 from the profile or re-oxidized to Fe(III) oxides upon re-oxygenation of the soil (Wang et al., 2017). While redox-mediated transformations of Fe(III) oxides and export of Fe(II) is a well-known phenomenon (“gleying”) in seasonally flooded soils (Chen et al., 2017), their impact on mineral-associated OM has yet to be determined. Further, Al oxides, rather than Fe oxides, are the predominate mineral phases contributing to OM retention in forested floodplain sediments because their solubility is controlled by pH rather than redox conditions (Darke and Walbridge, 2000), and may thus play a critical role in mineral  
10 protection in seasonally flooded soils.

Water saturation thus likely governs C cycling in seasonally flooded soils through its combined impact on oxygen availability, root dynamics and mineralogy; but how the relative contribution of these biogeochemical controls vary across spatial and temporal gradients is still unknown. A recent study along hillslope transects in tropical forest soils representing an oxygen gradient (Hall and Silver, 2015), for example, found that a combination of Fe (II) (a proxy for reducing conditions),  
15 fine root biomass, and total Fe and Al concentrations explained the most variation of surface soil C contents. How the relationships between C and important biogeochemical controls differ in systems that undergo longer, yet not permanent, periods of water saturation is still in question – especially with depth.

In this study, we aimed to identify the predominant environmental and biogeochemical controls on CO<sub>2</sub> efflux, C content, and OM composition in seasonally flooded mineral soils. To accomplish this goal, we studied the impact of seasonal  
20 flooding on C cycling across complete soil profiles (0 to 1 m) in six replicated upland-to-lowland transects typical for the Northeastern US (Brooks, 2005). Our objectives were to (i) identify the environmental parameters that drive temporal dynamics of CO<sub>2</sub> efflux in seasonally flooded soils and (ii) examine the relative importance of biogeochemical controls on C concentration and C chemistry with depth. To accomplish our first objective, we related soil CO<sub>2</sub> efflux at three landscape positions (upland, transition, and lowland) spanning the transect over the course of a full drainage and flooding cycle to  
25 measures of soil temperature, moisture, water table depth and redox potential. To accomplish our second objective, we



examined variations in C content and chemistry in both surface and subsurface horizons in relation to root distribution, mineralogy and redox potential. We hypothesized that seasonally reduced conditions upon flooding will result in lower CO<sub>2</sub> efflux, greater C accumulation, lower capacity of minerals to protect OM, and a selective preservation of macromolecular or chemically-reduced OM compared to the upland position. We anticipated that the transition position would represent an intermediate between upland and lowland positions.

## 2 Methods

### 2.1 Site description

Our study included six replicate forested wetlands in western Massachusetts that experience seasonal flooding through groundwater recharge; three sites are located at the UMass Experimental Farm Station in South Deerfield, MA, and three located within the Plum Brook Conservation area in South Amherst, MA. All sites consisted of soils that are glacially-derived sandy loams classified as mesic Typic Dystrudepts. Vegetation is dominated by red maple (*Acer rubrum*) and white oak (*Quercus alba*) stands with understory vegetation primarily composed of cinnamon fern (*Osmunda cinnamomea*), Canada mayflower (*Maianthemum canadense*), reed canary grass (*Phalaris arundinacea*), and jewelweed (*Impatiens capensis*). Mean annual air temperatures ranged from 8.8°C and mean annual precipitation is 1117 mm.

### 2.2 Field measurements

A transect in each seasonal wetland was delineated from an upland position to a lowland position (Fig. 1a-c). Three positions, termed “upland”, “transition”, and “lowland”, along each transect were established as monitoring stations and for soil sample collection. The upland position is in a forested landscape, approximately five meters away from the edge of the wetland, and does not undergo any flooding. The transition position is located on the edge of the wetland, which typically does not flood in an average rainfall year, but is under the influence of water table rise. The lowland position is in the lowest point of the wetland and is typically flooded for several months throughout the year. Horizons in the upland position were classified as A (0-25 cm), B (25-55 cm), and C (55-84+ cm) horizons; in the transition position as A (0-28 cm), C (28-48 cm), and Cg (48-69+); and in the lowland position as A (0-25 cm), C (25-35 cm), and Cg (35-68+ cm) (Soil Survey Staff, 1999) (Fig. 1a). Each landscape position was monitored for CO<sub>2</sub> emissions, soil temperature, volumetric moisture content (VMC) at 0 to 10



cm, water table depth, and  $E_h$ . Field measurements were collected weekly at each designated landscape position in all six seasonal wetlands from May through August, then monthly from September through April. A field portable automated gas flux analyzer (LI-8100A, LI-COR Biotechnology, Lincoln, NE) was used to measure rates of  $CO_2$  emissions, on permanently installed PVC collars, soil temperature and VMC. Three measurements of  $CO_2$  fluxes were taken at each individual PVC collar

5 using observation times of one minute, with 15 second dead band and pre- and post- purge times. The standard deviation of three observations was calculated in the field and a 15 % threshold was used for acceptable measurements. If the resulting standard deviation of the three measurements was greater than 15 % subsequent measurements were taken until the threshold was met. Based on other reports for comparable sites (Kifner et al. 2018), we expected methane production within these seasonal wetlands. However, in those sites methane production was 20-times lower than  $CO_2$  production. While we fully

10 acknowledge the disproportionate potency of methane as a climate-active greenhouse gas, our study aimed to determine the environmental and biogeochemical factors influencing C accrual or depletion in soils. We thus focused our monitoring efforts on quantitatively more important  $CO_2$  emissions as the predominant C loss pathway. Water table fluctuations were monitored using slotted PVC pipes installed to depths of 100 cm. Platinum-tipped  $E_h$  probes were installed in triplicate at each depth of 15-, 30-, and 45-cm; each group (nine) of  $E_h$  probes were accompanied with a single salt bridge filled with saturated KCl in

15 3% agar for the reference electrode. In total, each landscape position had 18 redox probes installed at each depth.  $E_h$  was measured using a calomel electrode (Fisher Scientific, Pittsburg, PA) attached to a voltmeter and corrected to a standard hydrogen electrode by adding 244 mV to each reading (Fiedler et al., 2007).

### 2.3 Soil sampling and analysis

Soil samples were collected from all sites, positions and horizons using hand-augers. Coarse rocks and roots were removed

20 from soil samples which were then sieved using standard 2 mm screens. Particle size distribution was determined using the pipette method outlined by Gee and Bauder (1986). Total C and N were determined with an elemental analyzer (Hedges and Stern, 1984). Extractable iron and aluminum concentrations were measured on each soil horizon from all three positions from the six pools ( $n=62$ ) using ammonium-oxalate and citrate-bicarbonate-dithionite (CBD) extraction procedures (Loeppert and Inskeep, 1996). Ammonium-oxalate extractable Fe ( $Fe_o$ ) and Al ( $Al_o$ ) represent the poorly crystalline pool of Fe, while the

25 CBD extractable Fe ( $Fe_d$ ) and Al ( $Al_d$ ) represent the total reducible Fe.



Root biomass was determined by taking soil cores in all six wetlands at each position along the designated moisture transects. The cores were taken at 0-20 cm, 20-40 cm, and >40 cm. Root biomass was determined using a USDA NRCS hand sieving method (Soil Survey Staff, 1999). The initial values of root biomass were used to determine biomass values for each soil horizon using an equal-area quadratic spline function (Spline Tool v2.0, ASRIS). Mean  $E_h$  values for each soil horizon were also estimated using the spline function.

To determine the relative abundance of specific C functional groups and degree of oxidation, soil samples were analyzed using C (1s) near edge X-ray absorption fine structure (NEXAFS) spectroscopy at the Canadian Light Source (CLS) in Saskatoon, Canada. Soil samples from individual horizons were gently ground, slurried in DI-H<sub>2</sub>O and pipetted onto clean In foils. After drying, C NEXAFS spectra were obtained using the spherical grating monochromator (SGM) beamline 11ID-1 (Regier, 2007). Step scan mode (0.25 eV steps from 270 to 320 eV) was used to minimize x-ray damage. A dwell time of 20 ms was used between scans. Individual spectra were collected at new locations on each sample for a total of 40 to 60 scans. The beamline exit slit was set at 25 mm, and the fluorescence yield data was collected using a two-stage microchannel plate detector. The resulting spectra were averaged for each sample and the averaged spectrum was then baseline normalized to zero and then normalized the beamline photon flux ( $I_0$ ) from a separate Au reference foil. Each spectrum was calibrated to the carboxylic acid peak (288.5 eV) of a citric acid standard. Pre-edge (270-278 eV) and post-edge (310-320 eV) and an  $E_0$  (290 eV) values were used to perform an edge step normalization. Peak deconvolution was conducted in Athena (Demeter version 0.9.25, 2006-2016); Ravel and Newville 2005) to determine the relative abundances of functional groups, with peak positions as described in Keiluweit et al. (2017). Gaussian peak positions, their full-width at half-maximum, and the arc tangent function were fixed. Peak height was set to vary freely during the fitting process. Parameters were adjusted until optimal fits for each spectrum were achieved and all spectra were fitted with these final parameters.

To determine the composition of bioavailable compounds that can potentially be used in microbial respiration (<600Da, Logue et al., 2016), water extracts of soil samples were collected on a 12 Tesla Bruker Solarix Fourier-transform ion cyclotron resonance mass spectrometer located at Environmental Molecular Sciences Laboratory (EMSL), a Department of Energy Biological and Environmental Research (DOE-BER) national user facility located in Richland, WA. Soil samples were extracted with ultrapure DI-H<sub>2</sub>O using one gram of soil and 10 mL of DI-H<sub>2</sub>O (1:10). The samples were sealed in 15 mL



conical tip tubes and shaken for one hour. Samples were then centrifuged and filtered using syringe-filters and the resulting filtrate solution was used for FT-ICR-MS analysis. A standard Bruker electrospray ionization (ESI) source was used to generate negatively charged molecular ions; samples were then introduced directly to the ESI source. The instrument was externally calibrated to a mass accuracy of  $<0.1$  ppm weekly using a tuning solution from Agilent, which contains the following

5 compounds:  $C_2F_3O_2$ ,  $C_6HF_9N_3O$ ,  $C_{12}HF_{21}N_3O$ ,  $C_{20}H_{18}F_{27}N_3O_8P_3$ , and  $C_{26}H_{18}F_{39}N_3O_8P_3$  with an  $m/z$  ranging between 112 to 1333. The instrument settings were optimized by tuning on a Suwannee River Fulvic Acid (SRFA) standard. Blanks (HPLC grade MeOH) were also ran at the beginning and the end of the day to monitor potential carry over from one sample to another. The instrument was flushed between samples using a mixture of water and methanol. The ion accumulation time (IAT) was varied to account for differences in C concentration between samples and varied between 0.1 and 0.3 s. Ninety-six individual

10 scans were averaged for each sample and internally calibrated using OM homologous series separated by 14 Da ( $-CH_2$  groups). The mass measurement accuracy was less than 1 ppm for singly charged ions across a broad  $m/z$  range (i.e.  $200 < m/z < 1200$ ). To further reduce cumulative errors, all sample peak lists for the entire dataset were aligned to each other prior to formula assignment to eliminate possible mass shifts that would impact formula assignment. Putative chemical formulas were assigned using Formularity software (Tolić et al., 2017). Chemical formulas were assigned based on the following criteria:  $S/N > 7$ , and

15 mass measurement error  $< 1$  ppm, taking into consideration the presence of C, H, O, N, S and P and excluding other elements. Peaks with large mass ratios ( $m/z$  values  $> 500$  Da) often have multiple possible candidate formulas. These peaks were assigned formulas through propagation of  $CH_2$ , O, and  $H_2$  homologous series. Additionally, to ensure consistent choice of molecular formula when multiple formula candidates are found the following rules were implemented: we consistently chose the formula with the lowest error with the lowest number of heteroatoms and the assignment of one phosphorus atom requires the presence

20 of at least four oxygen atoms. Peaks that were present in the blanks were subtracted from the sample data sets. Additionally, all single peaks i.e. peaks that are present in only one sample were removed and are not included in the downstream analysis. To further identify only “unique” peaks, we compared samples with the same group against each other to keep the peaks in the sample set that occur at least half of the samples for that group; peaks that occurred in less than half the samples were discarded from the final data set.



To visualize differences in SOM composition, compounds were plotted on a van Krevelen diagram corresponding to their H/C (hydrogen to carbon) vs. O/C (oxygen to carbon) ratios (Kim et al., 2003). Van Krevelen diagrams provide a way to visualize and compare the average properties of OM and assign compounds to the major biochemical classes (i.e., lipid-, protein-, lignin-, carbohydrate-, - and condensed aromatic-like) (Kim et al., 2003). To identify the degree of oxidation of the

5 SOM we calculated the nominal oxidation state of carbon (NOSC) (Keiluweit et al., (2017):

$$NOSC = -\left(\frac{-Z+4C+H-3N-2O+5P-2S}{C}\right) + 4 \quad (1)$$

in which C, H, N, O, P, and S correspond to stoichiometry values measured by FT-ICR-MS, and Z is equal to the net charge of the organic compound (assumed to be zero). We utilized the calculated double bond equivalent (DBE) to determine the degree of saturation of the identified C compounds, using the equation set forth by Koch and Dittmar (2006):

$$10 \quad DBE = 1 + \frac{1}{2}(2C - H + N + P) \quad (2)$$

where C, H, N, O, P, and S correspond to stoichiometry values also measured by FT-ICR-MS. The DBE is a useful equation to determine the degree of unsaturation of organic carbon containing molecules, where higher DBE values indicates less H atoms and a greater density of C-C double bonds. We also analyzed aromaticity of water extractable organic matter using a modified aromaticity index (AI<sub>mod</sub>) to determine the density of C-C double-bonds, using the amended equation by Koch and

15 Dittmar (2016):

$$AI_{mod} = \frac{1+C-\frac{1}{2}O-S-\frac{1}{2}(N+P+H)}{C-\frac{1}{2}O-N-S-P} \quad (3)$$

which takes into consideration the contributions of heteroatoms and  $\pi$ -bonds. To identify shifts in average molecular weights we calculated molecular weight using stoichiometry values measured by FT-ICR-MS:

$$MW = (C \times 12.011) + (H \times 1.008) + (O \times 15.999) + (S \times 32.06) + (P \times 30.974) + (N \times 14.007) \quad (4)$$

20 where each element is multiplied by its molar mass.

## 2.4 Statistical analyses

All statistical analyses and plots were done using Rstudio (Version 1.0.136, R Core Team 2015). The lm() function in Rstudio was used to perform linear regressions with the seasonal data to determine how various environmental parameters (soil moisture, water table depth and redox potential) predicted CO<sub>2</sub> emissions in the three landscape positions. Arrhenius



models were used to determine how soil temperature predicted CO<sub>2</sub> emissions in the three landscape positions using OriginPro (OriginLab) with the equation (Sierra et al. 2012):

$$k = Ae^{(-Ea/RT)} \quad (5)$$

where Ea is the activation energy, A is the pre-exponential factor, R is the universal gas constant (8.314 J K<sup>-1</sup> mol<sup>-1</sup>), and T is temperature in Kelvin (K). Relationships between total C and biogeochemical parameters were analyzed using linear mixed effects models with the lme4 package (Bates et al., 2015) in Rstudio. Two sets of mixed effects models were conducted; the first to identify which biogeochemical variables (root biomass, Fe<sub>o</sub>, Al<sub>o</sub>, clay, and redox) predicted C content in the different landscape positions where wetland number (n=6) was a random effect and horizon (A, B/C, C/Cg) and one additional predictor variable were fixed effects. The second set of models aimed at identifying how the same variables predicted soil C at different soil depths, where wetland number was chosen as a random effect and landscape position (upland, transition, lowland) and one additional predictor variable as fixed effects. The mixed effects models were performed individually with one fixed effect parameter in addition to the blocking factor of either horizon or landscape position. To correct for multiple testing effects, we used the Bonferroni correction factor where  $\alpha_{corrected}$  is equal to 0.01. Analyses were conducted on log transformed data when assumptions of normal distribution were not met. Analysis of variance (ANOVA) and Tukey's honestly significance difference tests were conducted in Rstudio.

### 3 Results

#### 3.1 Seasonal dynamics

Although our positions along the upland-to-lowland transect (i.e., upland, transition, lowland positions) are only a few meters apart each, we found significant differences in the seasonal dynamics of soil respiration, water table depth, moisture content and redox conditions (Fig. 2).

*Soil respiration.* CO<sub>2</sub> fluxes in each landscape position began to rise in May and peaked in September. Thereafter, CO<sub>2</sub> efflux in all positions gradually declined to a baseline level until November. CO<sub>2</sub> fluxes remained at that low baseline level through April (Fig 2a). Cumulative CO<sub>2</sub> emissions during the growing season substantially decreased across the upland-to-lowland transect (Table 1). Relative to the lowland position (24 mol CO<sub>2</sub> m<sup>-2</sup> year<sup>-1</sup>), cumulative CO<sub>2</sub> emissions were 38%



greater in the transition position ( $33 \text{ mol CO}_2 \text{ m}^{-2} \text{ year}^{-1}$ ), and 58% greater in the upland position ( $38 \text{ mol CO}_2 \text{ m}^{-2}$ ). This general difference became even more pronounced when cumulative  $\text{CO}_2$  emissions were normalized to C content, with the upland position showing greater emissions than both the transition (p-value  $< 0.001$ ; Tukey's HSD) and lowland (p-value  $< 0.001$ , Tukey's HSD) positions. In the non-growing season, the transition position registered the largest cumulative  $\text{CO}_2$  flux (20 mole  $\text{CO}_2 \text{ m}^{-2}$ ), but there were no noticeable differences between the upland and lowland positions (16 and 15 mole  $\text{CO}_2 \text{ m}^{-2}$ , respectively) (Table 1).

*Moisture dynamics.* As typical in seasonal wetlands in the Northeastern US (Brooks, 2005), the water table in all three positions was highest from January to July and lowest from August through December (Fig. 2b). The lowland position had the greatest fluctuations in water table depth; the water table rose above the ground surface from February through June and dropped below the ground surface from July through January (-2 to -42 cm) (Table S1). The water table in the transition and upland positions showed similar seasonal dynamics, but the water table was significantly lower in the lowland position throughout the year. VMC generally followed water table fluctuations, although with less seasonal variation (Fig. 2c). Soil moisture was consistently the greatest in the lowland position; during the growing season VMC was 20% greater than the upland position (p-value  $< 0.05$ ; Tukey's HSD), and 15% greater in the non-growing season (p-value  $< 0.05$ ; Tukey's HSD) (Table S1).

*Redox dynamics.* Redox potential ( $E_h$ ) values typically mirrored the hydrologic conditions of each landscape position, with the lowest values generally occurring from May to July and the highest values between October and February (Fig. 2d). The lowland position had the largest seasonal amplitude, with values of less than 100 mV between May and July and above 500 mV from October to December.  $E_h$  in the transition position only fell to values between 200 to 300 mV between May and July, and recovered to values near 600 mV by October. The  $E_h$  values at the upland position remained above 450 mV throughout the entire year at 15 cm depth, but reached 400 mV or lower at 30 and 45 cm depths from May to July.

### 3.3 Distribution of carbon, root biomass, and mineralogy

To identify how roots and mineralogy affected the distribution of C across the upland-to-lowland transect, we examined C concentrations in relation to root biomass, texture, extractable Fe and Al and  $E_h$  (Table 3). Along the upland-to-lowland transects, C concentrations in the surface horizons increased whereas concentrations in the subsurface horizons



decreased along the transect (Table 3). C concentrations in the lowland position topsoil were two and four times greater than the transition ( $p$ -value  $< 0.01$ ; Tukey's HSD) and upland positions subsoils ( $p$ -value  $< 0.001$ ; Tukey's HSD), respectively. In contrast, the subsoils in the upland positions had nearly double the C concentrations than the subsoils of the transition and lowland positions. Root biomass significantly decreased from the upland to the lowland positions (Table 3). The upland position had nearly 10-times the amount of root biomass as the lowland position in the surface and subsurface horizons. Silt and clay content increased from the upland to the lowland positions, particularly in the subsoil (+33%, Table 3).  $Fe_o$  decreased by nearly 50 % from the upland to lowland positions in the topsoil. However, in the subsoil  $Fe_o$  almost doubled from the upland to the lowland positions. The upland position had significantly more  $Al_o$  than the transition and lowland positions in all horizons ( $p < 0.001$ , ANOVA), and declined with depth in each landscape position.  $Fe_d$  and  $Al_d$  strongly followed the trends of  $Fe_o$  and  $Al_o$  (Table 3), thus we further limit our discussion to  $Fe_o$  and  $Al_o$ .

### 3.4 Linear mixed effects models between total carbon and biogeochemical parameters

To determine the relative influence of roots, mineralogy and  $E_h$  on C concentrations in each landscape position, we performed linear mixed effects models using total C as a response variable and root biomass, clay,  $Fe_o$ ,  $Al_o$  and mean  $E_h$  in the growing season as predictor variables with horizon as a blocking factor (Fig. 4a). The relative importance of the predictor variables changed across the upland-to-lowland transect. In the upland position,  $Fe_o$  was the strongest predictor with the largest F-value (17.31,  $p < 0.001$ ), followed by root biomass (13.31,  $p < 0.01$ ). In the transition and lowland position, however, only root biomass and particularly  $Al_o$  were significantly correlated with C ( $p < 0.01$ ; Table 4). The model results show that as the importance of redox-active  $Fe_o$  as a predictor for soil C concentrations became less important along upland-to-lowland transects, the importance of  $Al_o$  increased.

To identify the influence of the biogeochemical variables on soil C concentrations with soil depth, we performed linear mixed effects models on the different horizons, using landscape position as a blocking factor (Fig. 4b). In the A-horizon,  $E_h$  had the highest F-value and strongest correlation to C (6.31,  $p$ -value  $< 0.05$ ; Table S3). In the lowest horizons,  $Al_o$  was the only significant predictor variable in the models (F-value = 16.10,  $p$ -value  $< 0.01$ , Table S3). These results indicate that, among the tested biogeochemical variables,  $E_h$  has a predominant influence on C concentrations in the surface soils, while  $Al_o$  has the strongest effect on C concentrations at depth.



### 3.5 Carbon chemistry across upland-to-lowland transitions

To examine variations in C chemistry C along upland-to-lowland transects, we analyzed solid-phase and water-extractable OM. C (1s) NEXAFS spectra showed an overall increase in abundance of chemically-reduced, solid-phase C across the upland-to-lowland transects in the topsoil, but an opposite trend in the subsoil (Fig. 5a, Table S3). Aliphatic, aromatic and  
5 carboxylic C relative abundances were significantly different amongst the three landscape positions ( $p$ -value =  $<0.05$ , ANOVA). The relative abundance of chemically-reduced aliphatic and aromatic C increased from the upland to the lowland position in the surface horizons, but their contribution decreased along the same transect in the subsurface horizons (Fig. 5a). Chemically more oxidized carboxylic C decreased in the surface horizons from the upland to lowland position, yet increased slightly in the subsoil along the same transect. As a measure of the degree of oxidation, we calculated carboxylic-to-aromatic  
10 C ratios (Fig. 5b), with higher ratios indicating a greater degree of oxidation. In the topsoil, the ratio gradually decreased across the upland-to-lowland transects in the topsoils (Table S4). In the subsoil, the opposite trend was observed, and the ratio increased from the upland C horizons to the lowland Cg horizons (Table S4).

To assess changes in oxidation state and molecular weight of compounds more readily available for microbial respiration, water extracts of all samples were analyzed by FT-ICR-MS. While the nominal oxidation state of carbon (NOSC)  
15 did not change significantly, both the modified aromaticity index ( $AI_{mod}$ ) and the average molecular weight of the detected compounds showed significant and gradual increases across the upland-to-lowland transitions (Fig. 6a, Table S5). Paralleling that change, the relative contributions of lignin increased (+7%) and that of lipids decreases (-11%) across the transect (Fig. 6b, Table S5). In the subsoils, however, both  $AI_{mod}$  and average molecular weight did not change significantly (Fig. 6a, Table S6), while the relative abundance of lignin increased (+9%) and that of lipids decreased (-11%).

## 20 4 Discussion

Our results show how seasonal flooding affects redox conditions, root biomass, and mineralogy as well as their impact on CO<sub>2</sub> efflux, C accumulation, and C chemistry across the upland-to-lowland transects. Our results demonstrate that the factors regulating CO<sub>2</sub> emissions and C accumulation shift as predicted in surface soils along the upland-to-lowland transects.



However, in subsoils, the factors regulating C accumulation under seasonally flooded soils differed significantly from that in topsoils.

#### 4.1 Environmental parameters controlling CO<sub>2</sub> emissions

Our hypothesis that reducing conditions inhibit microbial respiration and thus reduce CO<sub>2</sub> emissions in seasonally flooded soil is supported by our seasonal field data. We found strong correlations between seasonal CO<sub>2</sub> emissions and VMC, water table depth, and E<sub>h</sub> in the seasonally flooded lowland positions of our study sites (Fig. 3). In the upland position, however, soil temperature explained the most variation in CO<sub>2</sub> emissions (Fig. 3a, Table 2). Our results indicate that CO<sub>2</sub> emissions are mainly controlled by soil temperature in upland soils, but in seasonally flooded soils, water saturation and the associated low redox potentials become more important factors.

Our results further showed that CO<sub>2</sub> efflux is strongly regulated by water saturation and associated redox conditions, but only at temperatures sufficient for microbial activity (Fig. 2, Table 2). E<sub>h</sub> in the lowland position were typically less than 100 mV during the growing season, but greater than 400 mV during a majority of the non-growing season (October through January) (Fig. 2d, Table S2). The difference in E<sub>h</sub> between the growing and non-growing season in the lowland position indicates that E<sub>h</sub> is partly driven by the effects of temperature on microbial consumption of oxygen. We found significantly lower cumulative CO<sub>2</sub> emissions in the lowland position. This disparity was most pronounced during the growing season (Table 1), where the lowlands showed 40 % lower CO<sub>2</sub> emissions than upland soils (Table 1). In the non-growing season, lowland and upland positions had near equal emissions (Table 1, Fig. 2a). These findings indicate that, although these seasonally flooded soils become oxygenated, the aerobic period occurs when low seasonal temperatures inhibit microbial activity. In other words, when these seasonally flooded soils experience drained periods with increased oxygen availability, aerobic respiration still remains limited due to low temperatures.

#### 4.2 Contrasting impacts of roots, mineralogy and redox on C along the upland-to-lowland transect

C concentrations in the lowland topsoil were nearly four-times greater than in the upland topsoil (Table 3), which are more likely caused by lower respiration rates (Fig. 2a) than by differences in C inputs. Given the proximity of our three positions and the flat topography, aboveground litter inputs can be considered equal across the transect. Moreover, if



belowground C inputs were responsible for the greater C concentrations, we would expect root biomass to be higher in lowland than in upland positions. In fact, the opposite was the case (Table 3). Our linear mixed effects model further showed that C concentration in the topsoils was inversely related to  $E_h$  across the upland-to-lowland transect (Fig. 4b). In other words, low  $E_h$  values (i.e., oxygen availability) coincided with high C concentrations in the surface soil, an observation consistent with findings by Hall and Silver (2015) in tropical surface soils. Hence, greater C concentrations in lowland topsoils are likely due to oxygen limitations rather than greater above or belowground C inputs.

Surprisingly, this relationship did not hold true in the subsoils, where our linear mixed effects model showed that  $E_h$  failed to predict C concentrations across the transect (Fig. 4b, Table S3). Lower C concentrations in lowland subsoils as compared to upland subsoils (Table 3) were likely a consequence of differences in root biomass. Root biomass in lowland subsoils was 10-times less than in upland subsoils (Table 3), a difference that can be attributed to restricted root growth under oxygen limitations (Tokarz and Urban, 2015). With roots recognized as primary C inputs belowground, especially in the subsoil (Rasse et al., 2005), the lack of root-derived C may explain the low C stocks in deeper lowland horizons. With limited C inputs at depth, microbial oxygen consumption resulting from heterotrophic respiration may not be sufficient to cause prolonged oxygen limitations (Keiluweit et al. 2016). These results suggest that the effect of oxygen limitations on C accumulation in seasonally flooded soils may be most pronounced in C-rich topsoils, and less so in C-depleted subsoils.

Contrasting trends between upland and lowland soils were also found for the relationship between C concentrations and the presence of reactive Fe and Al phases, which are known to contribute to C accumulation (Wagai and Mayer, 2007). The amount of  $Fe_o$  in lowland soils was significantly lower than in upland soils (Table 3), consistent with the loss of reactive Fe phases observed in flooded paddy soils (Hanke et al., 2012) and in gleyed forest soils (Fiedler and Kalbitz, 2003). Here, redox-active minerals such as Fe(III) oxides are frequently lost due to reductive dissolution under reducing conditions and subsequent translocation (Chen et al., 2017).  $E_h$  values measured in lowland soil during the flooded period are sufficiently low for Fe(III) oxide reduction (Fig. 2d), likely causing the depletion in  $Fe_o$  observed here. Consequently, our linear mixed effects model showed that  $Fe_o$  served as the strongest measured predictor variable for C in upland soils, yet  $Fe_o$  had no predictive power in lowland soils (Fig. 4a). In contrast, our linear mixed effects models show that the strength of the relationship of C with  $Al_o$  significantly increases across upland-to-lowland transitions (Fig. 4a). Mineral protection of C in seasonally reduced



soils may thus depend on non-reducible Al oxides. Together, our results indicate that C storage in upland soils relies upon both root inputs and the presence of Fe and Al oxides, whereas C accumulation in lowland soils is more strongly linked to Al oxides.

In sum, the seasonally flooded soils in our study had sufficiently long periods of reducing conditions to accumulate C in the topsoil relative to the well-drained upland soils. C accumulated in the lowland surface soils most likely due to oxygen  
5 limitations and in spite of lower root C inputs and lower abundance of reactive Fe and Al phases. However, subsoils in seasonally flooded lowlands had much lower C concentrations than in the uplands; here C accumulation appears to be owed to non-redox active Al phases, but is limited by the lack of root C inputs belowground and the absence of reactive Fe phases.

#### 4.3 Divergent controls on C composition in seasonally flooded top- and subsoils

We hypothesized that anaerobic periods during flooding of the lowland soils limit the depolymerization of larger  
10 macromolecular compounds and/or the microbial respiration of chemically-reduced OM (Keiluweit et al., 2016). Conversely, we expected the upland positions to contain smaller and chemically more oxidized OM as a result of consistently largely aerobic conditions. While prior studies have primarily focused on total C in surface soils (Hall and Silver, 2015), subsurface soils (Olshansky et al., 2018), or DOM (Rouwane et al., 2018), this work represents the first examination of the depth-resolved chemical characteristics of C composition across upland-to-lowland transitions. Analysis of the composition of solid-phase  
15 and water-extractable C supported our predictions of a greater abundance of higher-molecular weight, chemically-reduced OM in the lowland positions, but only in the topsoil (Fig. 5, Fig. 6). Solid-phase OM across the upland-to-lowland transects became relatively enriched in reduced aromatic C and relatively depleted in oxidized carboxylic C in the topsoil (Fig. 5a). Water extractable OM of the lowland topsoils showed greater average molecular weight, higher aromaticity and higher contributions from lignin compounds compared to the upland topsoils (Fig. 6a,b). The fact that we observed only modest decreases in C  
20 oxidation state (Fig. 5b, Table S5) suggest thermodynamic limitations on microbial respiration (Keiluweit et al. 2017; Boye et al., 2017) play a limited role in topsoils. Instead, the fact that lignin-rich, aromatic, higher-molecular weight OM preferentially accumulates indicates that limited oxidative depolymerization of plant-derived OM under anaerobic conditions is primarily responsible for C accumulation in seasonally flooded topsoils.

Contrary to our expectation, subsoils showed the reverse trend and solid-phase C became significantly more oxidized  
25 along the upland-to-lowland transect (Fig. 5). Enhanced C oxidation in seasonally flooded soils is consistent with reports by



Olshanksky et al. (2018), who showed that wet-dry cycles increased the interactions between more oxidized OM constituents (i.e. carboxylic C) and soil minerals. It is also well known that subsoils in seasonally flooded soils receive significant amounts of dissolved OM leaching down from the topsoil (Fiedler and Kalbitz, 2003). Generally, the lowland positions of our study showed a decline in Fe<sub>o</sub> and Al<sub>o</sub> compared to the upland positions, but the lowland subsoil (Cg-horizon) showed an uptick in  
5 Fe<sub>o</sub> (Table 3). Such reactive Fe phases could potentially trap partially-oxidized, soluble compounds leaching down the profile and so result in the accumulation of relatively oxidized OM in seasonally flooded subsoils.

Additionally, changes in C oxidation state in subsoils may be driven by variations in root C inputs along the upland-to-lowland transect (Table 3). Root C inputs are composed of chemically reduced aliphatic (e.g. suberin and cutin) and aromatic compounds (e.g. lignin and tannins) (Spielvogel et al., 2014). With root biomass in upland positions being noticeably higher,  
10 such root-derived inputs may have resulted in greater contributions of chemically reduced OM (Liang and Balsler, 2008). In contrast, the lowland subsoils were nearly void of roots (Table 3). If OM in lowland subsoils predominantly stems from dissolved, oxidized OM leaching down the profile, as discussed above, the lack of root-derived, reduced OM compounds may result in an average C oxidation state that is relatively more oxidized.

#### 4.4 Balance between mineral and redox controls will determine response of seasonally flooded mineral soils to climate 15 change

Our results indicate that oxygen limitations are a significant control on C accumulation in seasonally flooded mineral soils. Warmer temperatures and less rain in the summer months is predicted to shorten the duration and alter the timing of flooding throughout the Northeastern US (Brooks, 2005). Consequently, seasonally flooded soils will likely become more oxygenated, lifting metabolic constraints on OM depolymerization and respiration, and promoting soil C loss and greater CO<sub>2</sub>  
20 emissions. Additionally, seasonal flooding over pedologic time scales has resulted in a loss of reactive minerals and metals and thus diminished the potential capacity of the soils to accumulate C through other means. Recent studies suggest that colonization by deep-rooting upland plants will offset some of the C loss upon drainage of former wetlands through additional C inputs (Gorham et al., 1991; Lal 2008). The lack of reactive metal phases observed in seasonally flooded soils investigated here suggests a low capacity for new C inputs to associate with reactive Fe or Al phases, and, consequently, a low potential to  
25 offset the losses of anaerobically protected C upon drainage.



## 5 Conclusions

Our examination of CO<sub>2</sub> emissions, C concentrations, and organic matter composition across six-replicated upland-to-lowland transects yielded important insights into the controls on C cycling in seasonally flooded soils. Importantly, we see distinctly different mechanisms controlling C concentration and organic matter composition in surface versus subsurface soils, which sharply contrasts those governing the upland system. While Fe<sub>o</sub> and Al<sub>o</sub> predicted C concentrations at the upland sites, E<sub>h</sub> and Al<sub>o</sub> best explained the significantly larger C accumulation in lowland soils. In spite of seasonal re-oxygenation of the topsoils, periodic flooding (and the associated oxygen limitations) imposed sufficient metabolic constraints on depolymerization and respiration to cause the accumulation of plant-derived, aromatic, high-molecular weight OM in topsoils. In the subsoil of seasonally flooded soils, anaerobic protection of C appears to be less important. C accumulation was low and primarily related to Al<sub>o</sub>, and the OM preserved at depth was relatively oxidized. The fact that anaerobic periods during flooding restricted root growth and caused a relative depletion of Fe(III) oxides in the subsoil suggests that the lack of root C inputs and reactive mineral surfaces are primarily responsible for the low subsurface C accumulation. Our findings suggest that anaerobically protected C in seasonally flooded surface soils may be particularly vulnerable to increased frequency of droughts. The extent to which associated C losses from surface soils may be compensated by upland plant encroachment and deeper root growth warrants further research.

## Acknowledgments

The authors thank T Regier, J Dynes, and Z Arthur for their assistance and support at the CLS SGM beamline 11ID-1. Research described in this paper was performed at the Canadian Light Source, which is supported by the Canada Foundation for Innovation, Natural Sciences and Engineering Research Council of Canada, the University of Saskatchewan, the Government of Saskatchewan, Western Economic Diversification Canada, the National Research Council Canada, and the Canadian Institutes of Health Research. The authors also thank A Thompson and C Brislawn (EMSL) for their technical help. The research was performed using EMSL, a DOE Office of Science User Facility sponsored by the Office of Biological and Environmental Research. Work conducted by REL was supported by the USDA National Institute of Food and Agriculture



(Hatch project 1007650). This work was supported by the Department of Energy, Office of Biological and Environmental Research, Subsurface Biosphere Research program (Award no. DE-SC0016544)

## References

- 5 ASRIS, ASRIS: Australian Soil Resource Information System., <http://www.asris.csiro.au>. Accessed September, 2016.
- Bates, D., Maechler, M., Bolker, B., Walker, S., Bojesen, R. H., Singmann, H., Dai, B., Scheipl, F., Grothendieck, G., and Green, P. lme4: Fitting Linear Mixed-Effects Models Using lme4. *Journal of Statistical Software*, 67(1), 1-48. doi:10.18637/jss.v067.i01, 2015.
- Boye, K., Noël, V., Tfaily, M. M., Bone, S. E., Williams, K. H., Bargar, J. R. and Fendorf, S.: Thermodynamically controlled  
10 preservation of organic carbon in floodplains, *Nature Geoscience*, 10(6), 415–419, doi:[10.1038/ngeo2940](https://doi.org/10.1038/ngeo2940), 2017.
- Bradford, M. A., Keiser, A. D., Davies, C. A., Mersmann, C. A. and Strickland, M. S.: Empirical evidence that soil carbon formation from plant inputs is positively related to microbial growth, *Biogeochemistry*, 113(1–3), 271–281, doi:[10.1007/s10533-012-9822-0](https://doi.org/10.1007/s10533-012-9822-0), 2013.
- Bridgman, S. D., Patrick Megonigal, J., Keller, J. K., Bliss, N. B. and Trettin, C.: The carbon balance of North American  
15 wetlands, *Wetlands*, 26(4), 889–916, 2006.
- Brooks, R. T.: A review of basin morphology and pool hydrology of isolated ponded wetlands: implications for seasonal forest pools of the northeastern United States, *Wetlands ecology and management*, 13(3), 335–348, 2005.
- Chen, C., Kukkadapu, R. K., Lazareva, O. and Sparks, D. L.: Solid-Phase Fe Speciation along the Vertical Redox Gradients in Floodplains using XAS and Mössbauer Spectroscopies, *Environmental Science & Technology*, 51(14), 7903–7912,  
20 doi:10.1021/acs.est.7b00700, 2017.
- Cohen, M. J., Creed, I. F., Alexander, L., Basu, N. B., Calhoun, A. J. K., Craft, C., D’Amico, E., DeKeyser, E., Fowler, L., Golden, H. E., Jawitz, J. W., Kalla, P., Kirkman, L. K., Lane, C. R., Lang, M., Leibowitz, S. G., Lewis, D. B., Marton, J., McLaughlin, D. L., Mushet, D. M., Raanan-Kiperwas, H., Rains, M. C., Smith, L. and Walls, S. C.: Do geographically isolated wetlands influence landscape functions?, *Proceedings of the National Academy of Sciences*,  
25 113(8), 1978–1986, doi:10.1073/pnas.1512650113, 2016.



- Darke, A. K. and Walbridge, M. R.: Al and Fe Biogeochemistry in a floodplain forest: Implications for P retention, *Biogeochemistry*, 51(1), 1-32, 2000.
- Day, F. P. and Megonigal, J. P.: The relationship between variable hydroperiod, production allocation, and belowground organic turnover in forested wetlands, *Wetlands*, 13(2), 115–121, doi:[10.1007/BF03160871](https://doi.org/10.1007/BF03160871), 1993.
- 5 Fenner, N. and Freeman, C.: Drought-induced carbon loss in peatlands, *Nature Geoscience*, 4(12), 895–900, doi:[10.1038/ngeo1323](https://doi.org/10.1038/ngeo1323), 2011.
- Fiedler, S., and Kalbitz., K.: Concentrations and Properties of Dissolved Organic Matter in Forest Soils as Affected by the Redox Regime, *Soil Science*, 168(11), 793-801, 2003.
- Fiedler, S., Vepraskas, M. J. and Richardson, J. L.: Soil Redox Potential: Importance, Field Measurements, and Observations, in *Advances in Agronomy*, vol. 94, pp. 1–54, Elsevier., 2007.
- 10 Gee, G. W., and Bauder, J. W.: Particle Size Analysis, *Methods of Soil Analysis, Part A*. Klute (ed.). 2 Ed., Vol. 9 nd. Am. Soc. Agron., Madison, WI, pp: 383-411, 1986.
- Gorham, E.: Northern Peatlands: Role in the Carbon Cycle and Probable Responses to Climatic Warming, *Ecological Applications*, 1(2), 182–195, doi:[10.2307/1941811](https://doi.org/10.2307/1941811), 1991.
- 15 Hall, S. J. and Silver, W. L.: Reducing conditions, reactive metals, and their interactions can explain spatial patterns of surface soil carbon in a humid tropical forest, *Biogeochemistry*, 125(2), 149–165, doi:[10.1007/s10533-015-0120-5](https://doi.org/10.1007/s10533-015-0120-5), 2015.
- Hanke, A., Sauerwein, M., Kaiser, K. and Kalbitz, K.: Does anoxic processing of dissolved organic matter affect organic–mineral interactions in paddy soils?, *Geoderma*, 228–229, 62–66, doi:[10.1016/j.geoderma.2013.12.006](https://doi.org/10.1016/j.geoderma.2013.12.006), 2014.
- Hedges, J. I. and Stern, J. H.: Carbon and nitrogen determinations of carbonate-containing solids<sup>1</sup>, *Limnology and Oceanography*, 29(3), 657–663, doi:10.4319/lo.1984.29.3.0657, 1984.
- 20 Jones, D. L., Nguyen, C. and Finlay, R. D.: Carbon flow in the rhizosphere: carbon trading at the soil–root interface, *Plant and Soil*, 321(1–2), 5–33, doi:[10.1007/s11104-009-9925-0](https://doi.org/10.1007/s11104-009-9925-0), 2009.
- Keiluweit, M., Nico, P. S., Kleber, M. and Fendorf, S.: Are oxygen limitations under recognized regulators of organic carbon turnover in upland soils?, *Biogeochemistry*, 127(2–3), 157–171, doi:[10.1007/s10533-015-0180-6](https://doi.org/10.1007/s10533-015-0180-6), 2016.



- Keiluweit, M., Wanzek, T., Kleber, M., Nico, P. and Fendorf, S.: Anaerobic microsites have an unaccounted role in soil carbon stabilization, *Nature Communications*, 8(1), doi:[10.1038/s41467-017-01406-6](https://doi.org/10.1038/s41467-017-01406-6), 2017.
- Kifner, L. H., Calhoun, A. J. K., Norton, S. A., Hoffmann, K. E. and Amirbahman, A.: Methane and carbon dioxide dynamics within four vernal pools in Maine, USA, *Biogeochemistry*, 139(3), 275–291, doi:[10.1007/s10533-018-0467-5](https://doi.org/10.1007/s10533-018-0467-5), 2018.
- 5 Kim, S., Kramer, R. W. and Hatcher, P. G.: Graphical Method for Analysis of Ultrahigh-Resolution Broadband Mass Spectra of Natural Organic Matter, the Van Krevelen Diagram, *Analytical Chemistry*, 75(20), 5336–5344, doi:[10.1021/ac034415p](https://doi.org/10.1021/ac034415p), 2003.
- Kirwan, M. L. and Blum, L. K.: Enhanced decomposition offsets enhanced productivity and soil carbon accumulation in coastal wetlands responding to climate change, *Biogeosciences*, 8(4), 987–993, doi:[10.5194/bg-8-987-2011](https://doi.org/10.5194/bg-8-987-2011), 2011.
- 10 Koch, B. P. and Dittmar, T.: From mass to structure: an aromaticity index for high-resolution mass data of natural organic matter, *Rapid Communications in Mass Spectrometry*, 20(5), 926–932, doi:[10.1002/rcm.2386](https://doi.org/10.1002/rcm.2386), 2006.
- Koch, B. P. and Dittmar, T.: From mass to structure: an aromaticity index for high-resolution mass data of natural organic matter, *Rapid Communications in Mass Spectrometry*, 30(1), 250–250, doi:[10.1002/rcm.7433](https://doi.org/10.1002/rcm.7433), 2016.
- Koh, H.-S., Ochs, C. A. and Yu, K.: Hydrologic gradient and vegetation controls on CH<sub>4</sub> and CO<sub>2</sub> fluxes in a spring-fed  
15 forested wetland, *Hydrobiologia*, 630(1), 271–286, doi:[10.1007/s10750-009-9821-x](https://doi.org/10.1007/s10750-009-9821-x), 2009.
- Krauss, K. W. and Whitbeck, J. L.: Soil Greenhouse Gas Fluxes during Wetland Forest Retreat along the Lower Savannah River, Georgia (USA), *Wetlands*, 32(1), 73–81, doi:[10.1007/s13157-011-0246-8](https://doi.org/10.1007/s13157-011-0246-8), 2012.
- Laine, J., Silvola, J., Tolonen, K., Alm, J., Nykänen, H., Vasander, H., Sallantausta, T., Savolainen, I., Sinisalo, J. and Martikainen, P. J.: Effect of water-level drawdown on global climatic warming: Northern peatlands, *Ambio*, 179–184,  
20 1996.
- Lal, R.: Carbon sequestration, *Philosophical Transactions of the Royal Society B: Biological Sciences*, 363(1492), 815–830, doi:[10.1098/rstb.2007.2185](https://doi.org/10.1098/rstb.2007.2185), 2008.
- LaRowe, D. E. and Van Cappellen, P.: Degradation of natural organic matter: A thermodynamic analysis, *Geochimica et Cosmochimica Acta*, 75(8), 2030–2042, doi:[10.1016/j.gca.2011.01.020](https://doi.org/10.1016/j.gca.2011.01.020), 2011.



- Letey, J., and Stolzy, L.H. (1964) Measurement of Oxygen Diffusion Rates with the Platinum Microelectrode. *Hilgardia* 35: 545-554.
- Liang, C. and Balsler, T. C.: Preferential sequestration of microbial carbon in subsoils of a glacial-landscape toposequence, Dane County, WI, USA, *Geoderma*, 148(1), 113–119, doi:[10.1016/j.geoderma.2008.09.012](https://doi.org/10.1016/j.geoderma.2008.09.012), 2008.
- 5 Lloyd, J. and Taylor, J. A.: On the Temperature Dependence of Soil Respiration, *Functional Ecology*, 8(3), 315, doi:[10.2307/2389824](https://doi.org/10.2307/2389824), 1994.
- Loeppert, R. H., Inskeep, W.P.: *Methods of Soil Analysis. Part 3. Chemical Methods: Iron*. Soil Science Society of America and American Society of Agronomy, Madison, WI, USA, 639-644, 1996.
- Logue, J. B., Stedmon, C. A., Kellerman, A. M., Nielsen, N. J., Andersson, A. F., Laudon, H., Lindström, E. S. and Kritzberg, E. S.: Experimental insights into the importance of aquatic bacterial community composition to the degradation of dissolved organic matter, *The ISME Journal*, 10(3), 533–545, doi:[10.1038/ismej.2015.131](https://doi.org/10.1038/ismej.2015.131), 2016.
- 10 Megonigal, J.P., Hines, M.E., Visscher, P.T.: Anaerobic Metabolism: Linkages to Trace Gases and Aerobic Processes, in: Holland, H.D., Turekian, K.K. (Eds.), *Treatise on Geochemistry*. Pergamon, Oxford, pp. 317–424, 2003.
- Mitsch, W. J., Bernal, B., Nahlik, A. M., Mander, Ü., Zhang, L., Anderson, C. J., Jørgensen, S. E. and Brix, H.: Wetlands, carbon, and climate change, *Landscape Ecology*, 28(4), 583–597, doi:[10.1007/s10980-012-9758-8](https://doi.org/10.1007/s10980-012-9758-8), 2013.
- 15 National Centers for Environmental Information, National Oceanic and Atmospheric Administration, <https://www.ncei.noaa.gov>, last access: May 2018.
- Neckles, H. A. and Neill, C. Hydrologic controls of litter decomposition in seasonally flooded prairie marshes, *Hydrobiologia* 286: 155, doi:[10.1007/BF00006247](https://doi.org/10.1007/BF00006247), 1994.
- 20 Olshansky, Y., Root, R. A. and Chorover, J.: Wet–dry cycles impact DOM retention in subsurface soils, *Biogeosciences*, 15(3), 821–832, doi:[10.5194/bg-15-821-2018](https://doi.org/10.5194/bg-15-821-2018), 2018.
- Origin. 2003. Origin 7.5. OriginLab Corp., Northampton, MA.
- Rasse, D. P., Rumpel, C. and Dignac, M.-F.: Is soil carbon mostly root carbon? Mechanisms for a specific stabilisation, *Plant and Soil*, 269(1–2), 341–356, doi:[10.1007/s11104-004-0907-y](https://doi.org/10.1007/s11104-004-0907-y), 2005.
- 25 Ravel, B. and Newville, M.: ATHENA , ARTEMIS , HEPHAESTUS : data analysis for X-ray absorption spectroscopy using IFEFFIT, *Journal of Synchrotron Radiation*, 12(4), 537–541, doi:[10.1107/S0909049505012719](https://doi.org/10.1107/S0909049505012719), 2005.



- Regier, T., Krochak, J.K., Sham, T., Hu, Y.F., Thompson, J., and Blyth, R.I.R.: Performance and capabilities of the Canadian Dragon: The SGM beamline at the Canadian Light Source. *Nuclear Instruments and Methods in Physics Research Section A: Accelerators, Spectrometers, Detectors and Associated Equipment*, 582, 93-95. [10.1016/j.nima.2007.08.071](https://doi.org/10.1016/j.nima.2007.08.071), 2007.
- 5 Rouwane, A., Grybos, M., Bourven, I., Rabiet, M., and Guibaud, G.: Waterlogging and soil reduction affect the amount and apparent molecular weight distribution of dissolved organic matter in wetland soil: a laboratory study, *Soil Research*, 56(1), 28-38, doi: [10.1071/SR16308](https://doi.org/10.1071/SR16308)
- RStudio Team (2016). RStudio: Integrated Development for R. RStudio, Inc., Boston, MA  
URL <http://www.rstudio.com/>.
- 10 Schumacher, M., Christl, I., Vogt, R. D., Bartmettler, K., Jacobsen, C., and Kretzschmar, R.: Chemical composition of aquatic dissolved organic matter in five boreal forest catchments samples in spring and fall seasons, *Biogeochemistry*, (80)3, 263-275, doi: [10.1007/s10533-006-9022-x](https://doi.org/10.1007/s10533-006-9022-x), 2006.
- Sierra, C. A.: Temperature sensitivity of organic matter decomposition in the Arrhenius equation: some theoretical considerations, *Biogeochemistry*, 108(1–3), 1–15, doi:[10.1007/s10533-011-9596-9](https://doi.org/10.1007/s10533-011-9596-9), 2012.
- 15 Soil Survey Staff. *Soil taxonomy: A basic system of soil classification for making and interpreting soil surveys*. 2nd edition. Natural Resources Conservation Service. U.S. Department of Agriculture Handbook 436, 1996.
- Solomon, D., Lehmann, J., Kinyangi, J., Liang, B., and Schäfer, T.: Carbon K-Edge NEXAFS and FTIR-ATR Spectroscopic Investigation of Organic Carbon Speciation in Soils, *Soil Sci. Soc. of America Journal*, 69(1), 107, doi: [10.2136/sssaj2005.0107dup](https://doi.org/10.2136/sssaj2005.0107dup), 2005.
- 20 Spielvogel, S., Prietzel, J., Leide, J., Riedel, M., Zemke, J. and Kögel-Knabner, I.: Distribution of cutin and suberin biomarkers under forest trees with different root systems, *Plant and Soil*, 381(1–2), 95–110, doi:[10.1007/s11104-014-2103-z](https://doi.org/10.1007/s11104-014-2103-z), 2014.
- Sutton-Grier, A. E., Keller, J. K., Koch, R., Gilmour, C. and Megonigal, J. P.: Electron donors and acceptors influence anaerobic soil organic matter mineralization in tidal marshes, *Soil Biology and Biochemistry*, 43(7), 1576–1583, doi:[10.1016/j.soilbio.2011.04.008](https://doi.org/10.1016/j.soilbio.2011.04.008), 2011.
- 25 Tiner, R. W.: Geographically isolated wetlands of the United States, *Wetlands*, 23(3), 494–516, 2003.



- Tokarz, E. and Urban, D.: Soil Redox Potential and its Impact on Microorganisms and Plants of Wetlands, *Journal of Ecological Engineering*, 16, 20–30, doi:[10.12911/22998993/2801](https://doi.org/10.12911/22998993/2801), 2015.
- Tolić, N., Liu, Y., Liyu, A., Shen, Y., Tfaily, M. M., Kujawinski, E. B., Longnecker, K., Kuo, L.-J., Robinson, E. W., Paša-  
Tolić, L. and Hess, N. J.: Formularity: Software for Automated Formula Assignment of Natural and Other Organic  
5 Matter from Ultrahigh-Resolution Mass Spectra, *Analytical Chemistry*, 89(23), 12659–12665,  
doi:[10.1021/acs.analchem.7b03318](https://doi.org/10.1021/acs.analchem.7b03318), 2017.
- Torn, M. S., Trumbore, S. E., Chadwick, O. A., Vitousek, P. M. and Hendricks, D. M.: Mineral control of soil organic carbon  
storage and turnover, *Nature*, 389(6647), 170–173, doi:[10.1038/38260](https://doi.org/10.1038/38260), 1997.
- Wagai, R. and Mayer, L. M.: Sorptive stabilization of organic matter in soils by hydrous iron oxides, *Geochimica et*  
10 *Cosmochimica Acta*, 71(1), 25–35, doi:[10.1016/j.gca.2006.08.047](https://doi.org/10.1016/j.gca.2006.08.047), 2007.
- Wang, B., Zha, T. S., Jia, X., Wu, B., Zhang, Y. Q. and Qin, S. G.: Soil moisture modifies the response of soil respiration to  
temperature in a desert shrub ecosystem, *Biogeosciences*, 11(2), 259–268, doi:[10.5194/bg-11-259-2014](https://doi.org/10.5194/bg-11-259-2014), 2014.
- Wang, Y., Wang, H., He, J.-S. and Feng, X.: Iron-mediated soil carbon response to water-table decline in an alpine wetland,  
*Nature Communications*, 8, 15972, doi:[10.1038/ncomms15972](https://doi.org/10.1038/ncomms15972), 2017.
- 15 Zhao, Q., Adhikari, D., Huang, R., Patel, A., Wang, X., Tang, Y., Obrist, D., Roden, E. E. and Yang, Y.: Coupled dynamics  
of iron and iron-bound organic carbon in forest soils during anaerobic reduction, *Chemical Geology*, 464, 118–126,  
doi:[10.1016/j.chemgeo.2016.12.014](https://doi.org/10.1016/j.chemgeo.2016.12.014), 2017.



## Figure Captions

**Figure 1. Illustration of upland-to-lowland transects in forested seasonal wetlands used for this study.** (a) Approximate distances and elevation change between landscape positions along the transects as well as the horizons sampled within each position. Approximate seasonal high and low water table depths are indicated by dashed lines. Example of (b) flooded and (c) drained seasonal wetland with marked upland (U), transition (T) and lowland (L) positions.

**Figure 2. CO<sub>2</sub> efflux, water table, moisture and redox dynamics along upland-to-lowland transects.** Mean monthly (a) soil CO<sub>2</sub> efflux, (b) water table depths, (c) volumetric moisture contents, and (d) depth-resolved redox potentials for the three landscape positions; upland, transition and lowland. Redox potentials are standardized from a calomel to a hydrogen electrode. Data are the means of measurements along upland-to-lowland transects in six replicate wetlands.

**Figure 3. Pairwise linear regressions between soil CO<sub>2</sub> efflux and soil temperature, water table depth, moisture content and redox potential.** Monthly averages for each environmental variable, recorded in six replicate upland-to-lowland transects over a full year, were combined for regression analyses. Regression analyses were conducted for both growing (red-scale markers) and non-growing season (blue-scale markers). (a) Relationship between soil temperature at 10 cm depth and soil respiration modeled using the Arrhenius equation. (b) Linear regressions of water table depths against CO<sub>2</sub> efflux. Water table depths less than zero are below soil surface; depths greater than zero are above soil surface. (c) Linear regression of volumetric moisture contents at 10 cm depth plotted against CO<sub>2</sub> efflux. (d) Linear regressions of soil redox potentials at 15 cm depth plotted against CO<sub>2</sub> efflux. Growing season (GS) and non-growing season (NGS) fits are shown for each regression.

**Figure 4. Fixed effect parameters predicting total C in linear mixed effects models.** (a) F-values of fixed effects for Al<sub>o</sub>, Fe<sub>o</sub>, clay, root biomass, and mean growing season E<sub>h</sub> in each landscape position. (b) F-values of fixed effects for Al<sub>o</sub>, Fe<sub>o</sub>, clay, root biomass, and mean growing season E<sub>h</sub> in the different horizons.

**Figure 5. C (1s) NEXAFS analyses of solid-phase OM chemistry across upland-to-lowland transects.** (a) NEXAFS spectra from six replicate wetlands (grey), plotted for each landscape position and depth, with the resulting mean spectra plotted (black). Peaks of particular interest are carboxylic C (285.35 eV), aliphatic C (287.20 eV), and aromatic C (285.03 eV) denoted by dotted vertical lines. (b) Average carboxyl-to-aromatic C (285.35 eV/285.03 eV) ratios plotted for each landscape position and depth; bars are standard error of the mean of six replicates.

**Figure 6. FT-ICR-MS analysis of water-extractable OM chemistry across upland-to-lowland transects.** (a) Average relative abundances of compound classes as identified by O/C and H/C ratios in Krevelen plots. Grey-scale colors denoted



primarily plant-derived compound classes, while blue-scale compounds denote microbial-derived compound classes. (b) Average AImod values, as an index for aromaticity, and molecular weights of all detected compounds. Averages represent the mean of replicate samples from six upland-to-wetland transects; bars are standard error of the mean.



5

**Table 1 Average cumulative CO<sub>2</sub> emissions (n = 6 ± standard error) for each landscape position across upland-to-lowland transects**

	Full year mol CO <sub>2</sub> m <sup>-2</sup>	Growing season mol CO <sub>2</sub> m <sup>-2</sup>	Non-growing season mol CO <sub>2</sub> m <sup>-2</sup>	
Upland position	54 <sup>a</sup> ± 1.1	38 <sup>a</sup> ± 1.6	16 <sup>a</sup> ± 0.8	10
Transition position	53 <sup>a</sup> ± 0.9	33 <sup>a</sup> ± 1.5	20 <sup>a</sup> ± 0.9	
Lowland position	39 <sup>a</sup> ± 0.8	24 <sup>a</sup> ± 1.3	15 <sup>a</sup> ± 0.7	

Letter designations are Tukey's honestly significance test results. Different letter designations indicate a p-value of < 0.05.



**Table 2 Regression analysis (r) results of potential environmental variables that predict CO<sub>2</sub> emissions along a moisture gradient**

Environmental Variable	Season	Upland	Transition	Lowland
Soil temperature <sup>#</sup>	Full	0.72***	0.60***	0.53***
	GS	0.62***	0.56***	0.45***
	NGS	0.79***	0.81***	0.69***
Water Table Depth <sup>s</sup>	Full	-0.03	-0.05	-0.30**
	GS	-0.32**	-0.14	-0.55***
	NGS	-0.20	-0.17	-0.35**
Volumetric Moisture Content <sup>s</sup>	Full	0.20*	-0.44***	-0.32***
	GS	0.10	-0.72***	-0.51***
	NGS	-0.10	-0.37**	-0.37**
Soil Redox Potential <sup>s</sup>	Full	0.10	0.10	0.01
	GS	0.05	0.41***	0.40***
	NGS	0.06	0.08	0.27*

Full = entire year, GS = growing season, NGS = non-growing season.

<sup>#</sup> Arrhenius fit

<sup>s</sup> Linear fit

Significance codes: < 0.001 = '\*\*\*', 0.01 = '\*\*', 0.05 = '\*'

**Table 3 Average (n = 6 ± standard error) soil properties along the upland-to-lowland transect**

Horizon	Total Carbon (%)	C:N	Root Biomass (mg g <sup>-1</sup> soil)	pH	Silt + Clay (%)	Fe <sub>o</sub> (mg g <sup>-1</sup> soil)	Al <sub>o</sub> (mg g <sup>-1</sup> soil)
<b>Upland</b>							
A	2.3 <sup>ab</sup> ± 0.5	11 <sup>a</sup> ± 2.5	61 <sup>b</sup> ± 27	4.98 ± 0.2	48 <sup>a</sup> ± 11	3.6 <sup>b</sup> ± 0.5	5.1 <sup>c</sup> ± 0.8
B	1.1 <sup>ab</sup> ± 0.3	13 <sup>a</sup> ± 3.4	14 <sup>ab</sup> ± 3	5.22 <sup>a</sup> ± 0.2	39 <sup>a</sup> ± 11	2.4 <sup>ab</sup> ± 0.7	5.7 <sup>c</sup> ± 1.9
C	0.64 <sup>a</sup> ± 0.1	13 <sup>a</sup> ± 5.3	6 <sup>a</sup> ± 3	5.29 <sup>a</sup> ± 0.1	37 <sup>a</sup> ± 12	1.7 <sup>ab</sup> ± 0.4	3.6 <sup>abc</sup> ± 0.8
<b>Transition</b>							
A	3.9 <sup>bc</sup> ± 1.5	14 <sup>a</sup> ± 1.6	48 <sup>b</sup> ± 17	4.97 <sup>a</sup> ± 0.2	51 <sup>a</sup> ± 10	1.2 <sup>a</sup> ± 0.4	2.5 <sup>abc</sup> ± 0.3
B/C	0.64 <sup>a</sup> ± 0.1	6.4 <sup>a</sup> ± 1.4	15 <sup>ab</sup> ± 6	5.38 <sup>a</sup> ± 0.1	41 <sup>a</sup> ± 11	1.5 <sup>ab</sup> ± 0.3	1.9 <sup>abc</sup> ± 0.3
Cg	0.36 <sup>a</sup> ± 0.1	5.0 <sup>a</sup> ± 3.8	3 <sup>a</sup> ± 1	5.43 <sup>a</sup> ± 0.2	59 <sup>a</sup> ± 10	1.3 <sup>ab</sup> ± 0.3	1.3 <sup>ab</sup> ± 0.4
<b>Lowland</b>							
A	8.2 <sup>c</sup> ± 2.4	16 <sup>a</sup> ± 1.1	6 <sup>a</sup> ± 2	4.98 <sup>a</sup> ± 0.1	50 <sup>a</sup> ± 13	1.5 <sup>ab</sup> ± 0.4	4.1 <sup>bc</sup> ± 1.1
C	1.9 <sup>ab</sup> ± 0.5	13 <sup>a</sup> ± 3.7	2 <sup>a</sup> ± 0.6	5.29 <sup>a</sup> ± 0.1	66 <sup>a</sup> ± 9	1.0 <sup>a</sup> ± 0.3	2.6 <sup>abc</sup> ± 0.5
Cg	0.36 <sup>a</sup> ± 0.02	7.3 <sup>a</sup> ± 4.9	0.7 <sup>a</sup> ± 0.5	5.37 <sup>a</sup> ± 0.1	70 <sup>a</sup> ± 9	2.9 <sup>ab</sup> ± 0.7	1.0 <sup>a</sup> ± 0.2


**Table 4 Fixed effect parameters from the linear mixed models along the upland-to-lowland transects**

Variable	Degrees of freedom	Regression Coefficient $\pm$ standard error	F - value	Prob > F	Horizon Prob > F
<b>Upland</b>					
Root Biomass	17	0.15 $\pm$ 0.09	13.31	<0.01	NS
Fe <sub>o</sub>	17	0.37 $\pm$ 0.15	17.31	<0.001	NS
Al <sub>o</sub>	17	0.31 $\pm$ 0.09	10.76	<0.01	<0.05
Clay	17	0.39 $\pm$ 0.23	8.56	<0.01	<0.05
E <sub>h</sub>	17	0.24 $\pm$ 0.31	2.86	NS	<0.05
<b>Transition</b>					
Root Biomass	18	0.05 $\pm$ 0.07	21.81	<0.001	<0.05
Fe <sub>o</sub>	18	-0.05 $\pm$ 0.08	2.86	NS	<0.0001
Al <sub>o</sub>	18	0.14 $\pm$ 0.14	15.57	<0.001	<0.001
Clay	18	0.24 $\pm$ 0.07	1.68	NS	<0.0001
E <sub>h</sub>	18	-0.08 $\pm$ 0.08	0.32	NS	<0.0001
<b>Lowland</b>					
Root Biomass	12	0.12 $\pm$ 0.38	11.22	<0.01	NS
Fe <sub>o</sub>	12	-0.01 $\pm$ 0.17	0.45	NS	<0.01
Al <sub>o</sub>	12	0.91 $\pm$ 0.15	137.36	<0.0001	NS
Clay	12	-0.08 $\pm$ 0.21	0.31	NS	<0.01
E <sub>h</sub>	12	-0.47 $\pm$ 0.23	0.77	NS	<0.01

Model parameters with p-values > 0.05 are denoted as not-significant with the letters NS.

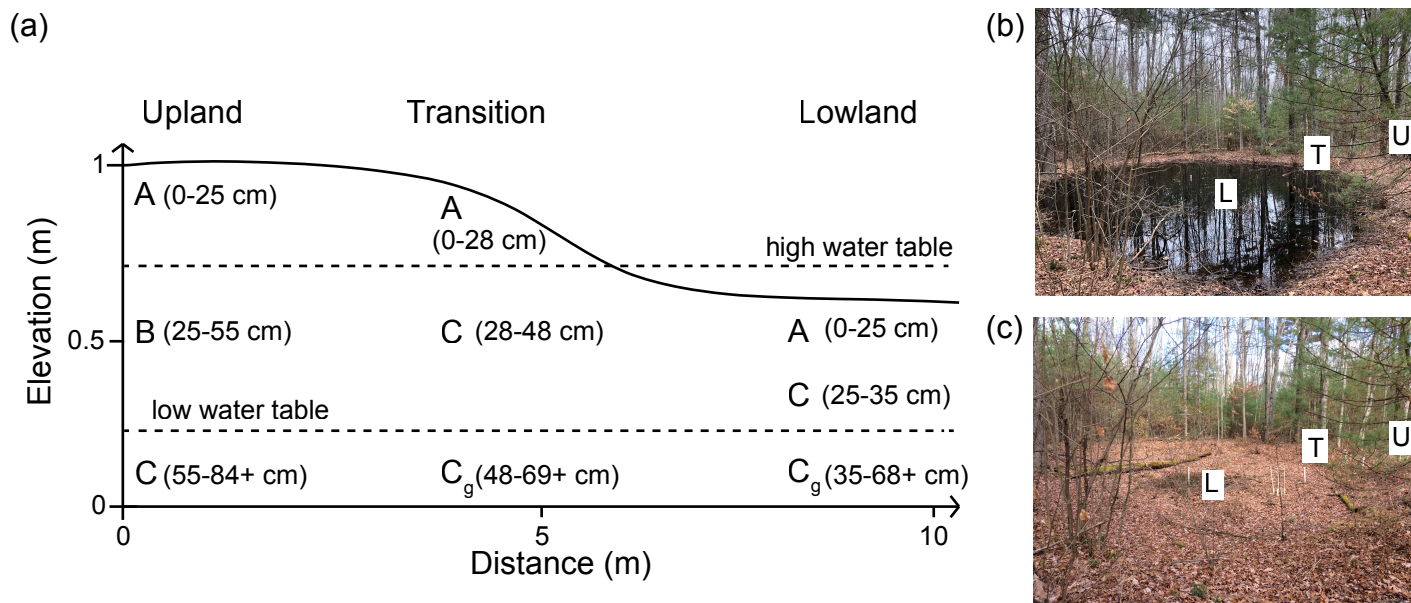


fig01

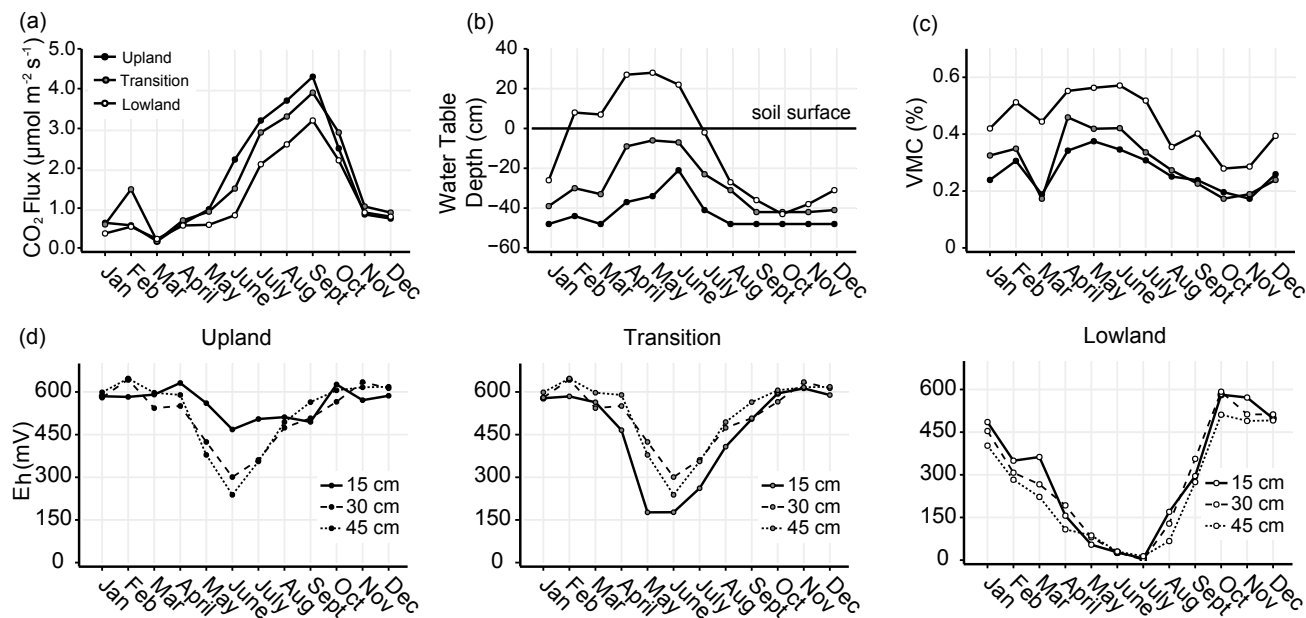


fig02

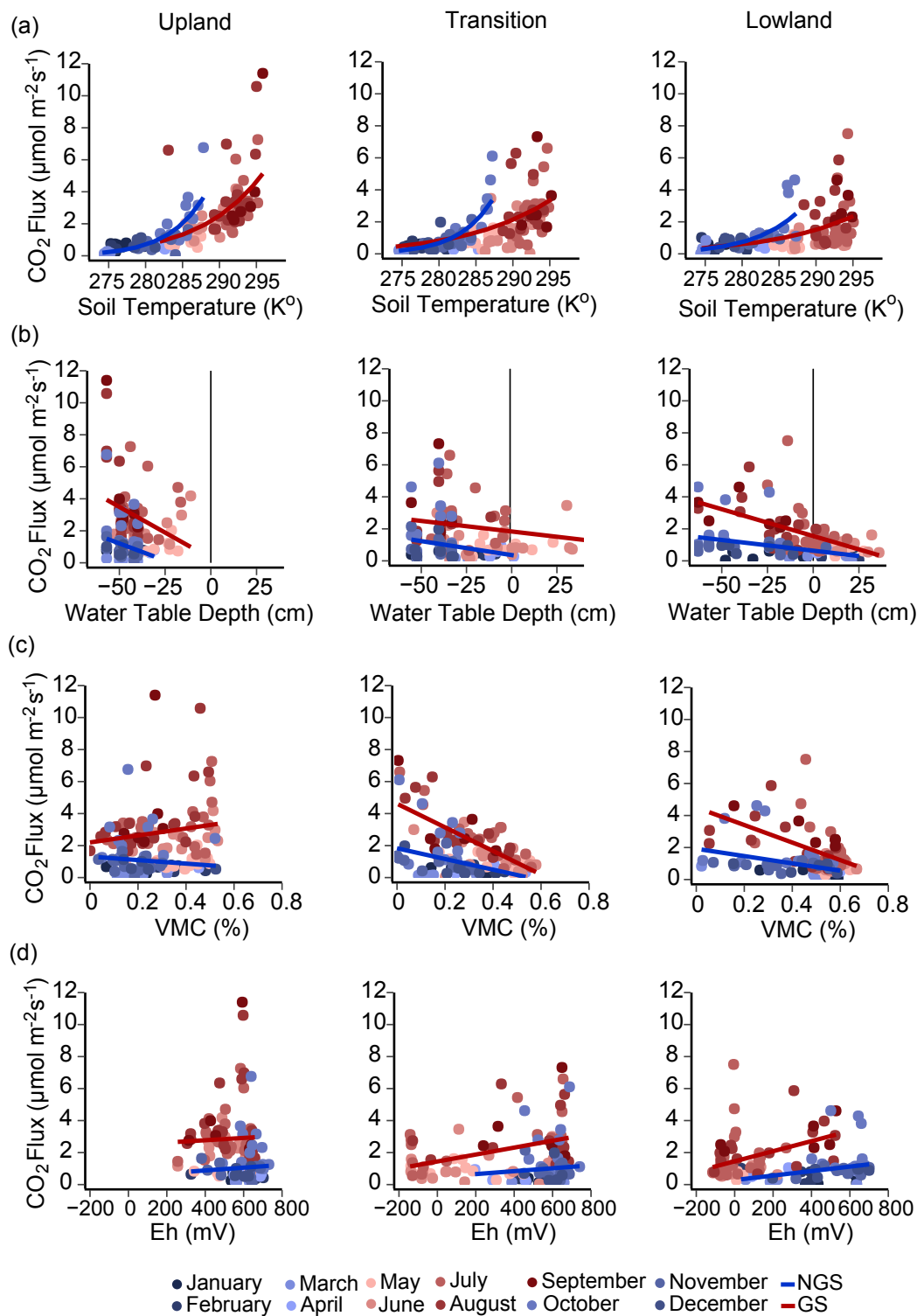


fig03

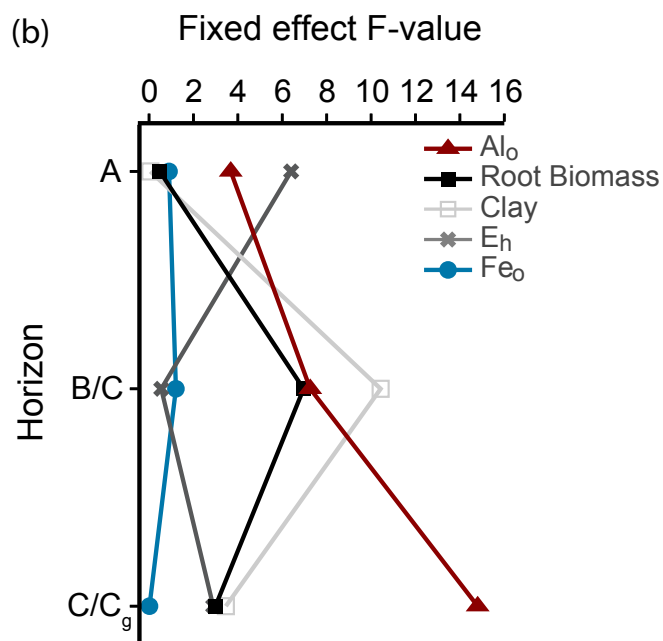
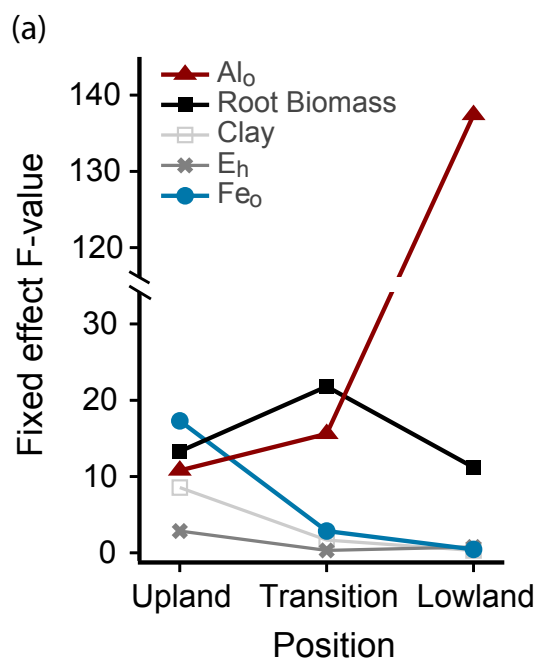


fig04

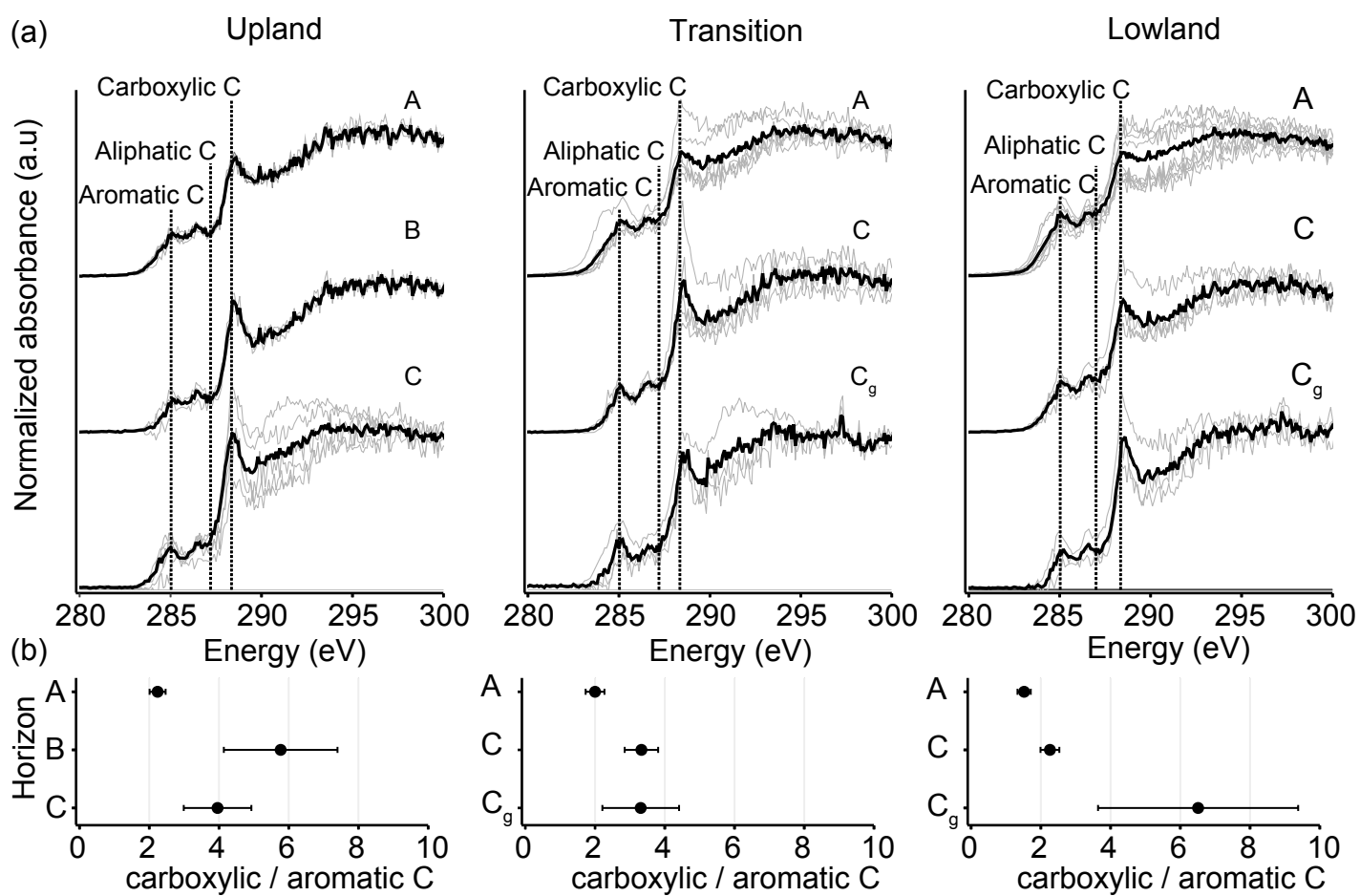


fig05

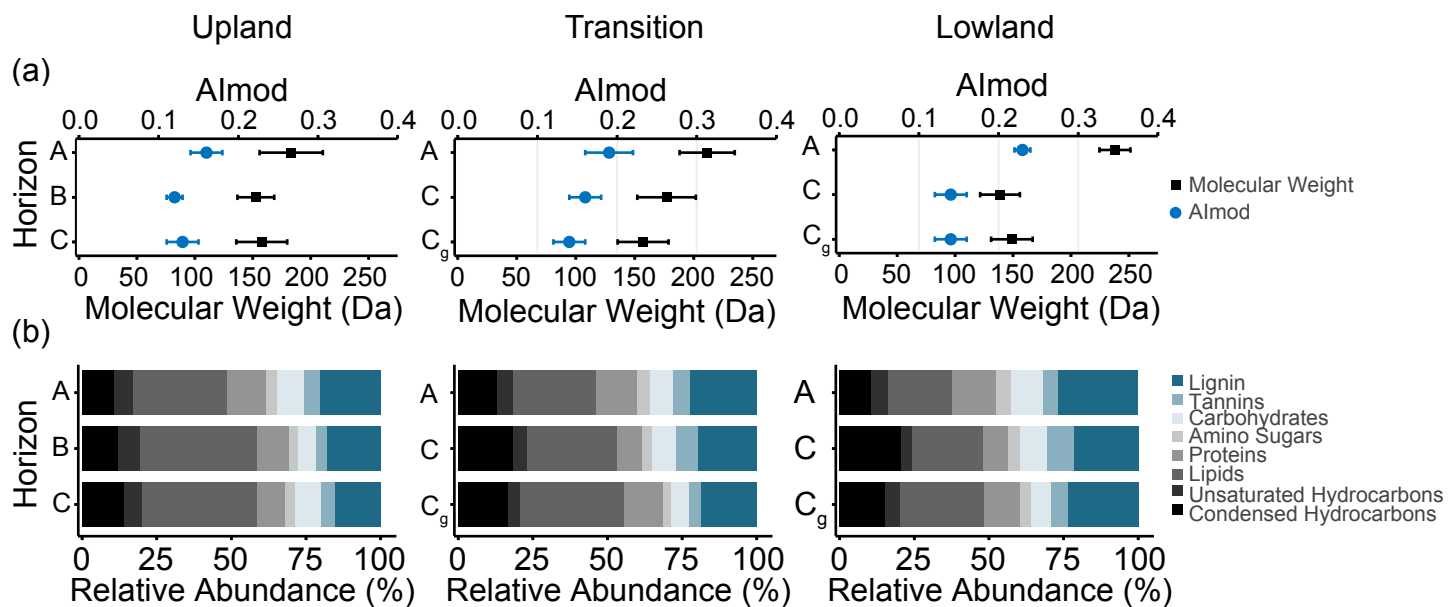


fig06